Heliyon 9 (2023) e22554

Contents lists available at ScienceDirect

Heliyon

journal homepage: www.cell.com/heliyon

Effect of temperature and glass content on crystalline phases in porcelain sintered with recovered automotive glass

A. Djemli [a,*], M.A. Ghebouli [b], K. Bouferrache [c], Y. Slimani [d], Mohamed A. Habila [e], Fatmi M [b,**], T. Chihi [b], B. Ghebouli [f], Mika Sillanpää [g]

[a] Faculty of Physics, University of Sciences & Technology Houari Boumediene (U.S.T.H.B), El Alia, BP 32, Bab Ezzouar, 16111, Algiers, Algeria
[b] Research Unit on Emerging Materials (RUEM), University Ferhat Abbas of Setif 1, Setif, 19000, Algeria
[c] Department of Physics, Faculty of Sciences, University of Mohamed Boudiaf, M'sila, 28000, Algeria
[d] Laboratory of Intelligent System (LSI), Faculty of Technology, University Ferhat Abbas of Setif 1, Setif, 19000, Algeria
[e] Department of Chemistry, College of Science, King Saud University, P.O. Box 2455, Riyadh, 11451, Saudi Arabia
[f] Laboratory for the Study of Surfaces and Interfaces of Solid Materials (LESIMS), University Ferhat Abbas of Setif 1, Setif, 19000, Algeria
[g] Department of Biological and Chemical Engineering, Aarhus University, Norrebrogade 44, 8000, Aarhus C, Denmark

ARTICLE INFO

Keywords:
Feldspars
Crystalline phases
Porcelain
Mullite

ABSTRACT

In the pursuit of sustainable porcelain production, this research examines the potential of using recovered automotive glass as a substitute for traditional feldspar, specifically feldspar imported from Spain. Porcelain samples were sintered at different temperatures and with varied proportions of automotive glass. The crystalline phases formed post-sintering were determined through X-ray diffraction and quantified by dissolving the porcelain in concentrated hydrofluoric acid. Results revealed that the inclusion of automotive glass, owing to its dissolved oxide content, accelerated the porcelain melting process and led to an increase in the vitreous phase. Notably, anorthite phases became dominant and mullite formation was evident at 1100 °C, stabilizing in samples G00 and G10, and then increasing at 1200 °C due to the emergence of secondary mullite. This secondary mullite forms from the residual silica after the primary mullite formation and the aluminium in the feldspars, which is about 17 %. For samples G20 and G30, only primary mullite was observed due to the decreased aluminium content resultant from feldspar replacement by glass. These findings underscore the viability of automotive glass in porcelain production, providing a sustainable and effective alternative to feldspar.

1. Introduction

From antiquity, ceramics for domestic use were predominantly produced from clay materials. However, it wasn't until the realization of their superior mechanical and thermal properties, which surpassed those of many metallic materials, that their application expanded [1]. Porcelain, a material absent in nature, emerges as a unique ceramic composite [2,3]. Due to its remarkable mechanical and thermal attributes, porcelain has intrigued numerous physicists and material scientists. Historical accounts suggest that "porcelain stone" played a pivotal role in the evolution of Chinese porcelain. This is attributed to the propensity of silicates to react readily with

* Corresponding author.
** Corresponding author.
E-mail addresses: amar.djemli@usthb.edu.dz (A. Djemli), fatmimessaoud@yahoo.fr (F. M).

https://doi.org/10.1016/j.heliyon.2023.e22554
Received 12 August 2023; Received in revised form 7 November 2023; Accepted 15 November 2023
Available online 23 November 2023

feldspars and kaolin at elevated temperatures, culminating in a homogeneous glassy matrix with enhanced translucency [4]. During the porcelain firing process, mineral components within the clay body engage in interactions, resulting in the formation of novel crystalline phases. Given the irreversible nature of these transformations, the resultant phases in the porcelain body serve as indicators of the zenith temperature the ceramic was exposed to. Such phase transitions are contingent upon factors such as temperature, mineralogical composition of the body, grain size, and the CO2 (or CO) content within the firing atmosphere [5,6]. X-ray diffraction stands out as an invaluable technique for delineating the crystalline phases inherent in porcelain, and is often employed to deduce firing temperatures [7]. For this study, the targeted phases to ascertain equivalent firing temperatures include quartz (SiO2) and mullite (3Al2O3·2SiO2). Kaolin clays, notably those with minimal CaO and alkali oxides content, are typified by mullite formation [8]. The kaolin, rich in alumina and silica, exhibits enhanced plasticity upon hydration. Beginning at 500 °C, kaolin undergoes dehydroxylation, shedding its hydroxyl groups to metamorphose into metakaolinite [9]. A temperature of 950 °C marks a structural loss in most kaolins, initiating the onset of high-temperature clay mineral alteration products, leading to the genesis of a spinel phase, 2Al2O3·3SiO2, and an amorphous phase [10]. Surpassing 1050 °C, this spinel, along with the amorphous phase, undergoes a transformation into mullite and cristobalite, enveloped within a silica-abundant glassy matrix [10,11]. Notably, studies [9] suggest the emergence of cristobalite and mullite at 1150 °C in kaolin-based clays, although traces of mullite become discernible as early as 1000 °C. In the presence of feldspars, which undergo melting between 1010 °C and 1100 °C, there is dissolution of cristobalite, promoting the formation of the ceramic's glassy phase that engulfs quartz crystals. At 1280 °C, the proliferation of large mullite crystals signifies a state with reduced viscosity where quartz dissolution occurs [10]. Hence, the detection of mullite implies a firing temperature of, at the very least, 1200 °C.

This study endeavours to elucidate the crystalline phases inherent in porcelain bodies when traditional feldspar is substituted with salvaged automotive glass and to quantify the porcelain's glassy phase percentage through acid dissolution. In order to identify the crystalline phases formed after the sintering process, we used an X-ray diffraction device. The phase transitions of porcelain are as follows: Kaolinite converts to metakaolin at 500–600 °C according to the following equation:

$$2AL_2(OH)_4Si_2O_5 \xrightarrow{600-500^\circ C} 2AL_2Si_2O_7 + 4H_2O$$

Feldspars begin to dissolve at 920 °C [10].

Metakaolin converts to spinel at 980 °C according to the following equation:

$$2Al_2Si_2O_7 \xrightarrow{980^\circ C} Al_4Si_3O_{12} + SiO_2$$

Spinel turns into primary mullite at 1100 °C according to the following equation:

$$3(Al_2O_3.2SiO_2) \xrightarrow{1100^\circ C} 3Al_2O_3.2SiO_2 + 4SiO_2$$

During the processing of samples at different temperatures and sintering times, several phase transformations occur that lead to: The decomposition of kaolin with partial dissolution of anorthite and quartz to form the liquid phase. The nuclei of the first mullite begin to nucleate and precipitate [10]. The primary mullite results from the reaction of aluminate and silica present in the metacaolinite, while the secondary mullite is produced from the added aluminium that reacts with the remaining silica from the transformation of the spinel (it does not appear on the x-rays because it is amorphous) into a primary mullite as well.

2. Sample preparation and characterization

For the preparation of porcelain samples, four primary raw materials were used: kaolin, quartz, feldspar, and glass. The kaolin, was sourced from Jebel Debbagh near Guelma, Algeria. Each raw material was subjected to a crushing process using a "pulverises" planetary ball mill. This milling continued for 5 h at a rotation speed of 250 rpm, utilizing zirconia balls of 15 mm diameter. As the crushing took place in water, a slurry mixture was formed. This slurry was subsequently dried in an oven at 150 °C for 24 h. The dried product was further manually crushed and sieved using a 150 μm mesh, ensuring a uniformly granulated powder. The sieved powders were compacted into a steel mold using a manual hydrostatic press capable of exerting a force of up to 15 tons. The resulting samples, consistent in diameter at 13 mm, were then subjected to various thermal treatments. Temperatures ranged from 1000 °C to 1300 °C at a stable heating rate of 10 °C/min, with sintering durations of 15, 30, 60, and 120 min. All treatments were carried out in a ST-1800 MX-III furnace, which can reach up to 1800 °C. For Characterization, JEOL JSM-6010LA Scanning Electron Microscopy and X-ray Diffraction (XRD) type PANalytical (ISM) with a Copper (Cu) X-ray tube, a common choice in XRD studies due to its efficiency in diffracting through a broad range of crystalline materials. The X-ray tube was operated at a voltage of 40 kV and a current of 30 mA. For our scans, we adopted a scanning speed of 2°/min, ensuring a balance between data acquisition time and resolution. Additionally, a step size of 0.01° was selected, were used to examine the microstructure of the alloy and to determine the elemental compositions of

Table 1
Components in the raw body.

Sample	wt. %
Kaolin	30–60
Quartz	10–40
Feldspar	25–35

the phases present in this simple. We chose a range of temperatures based on the known thermal behaviour of porcelain and its constituents. For instance, transformations such as Kaolinite to metakaolinite at 500–600 °C and Feldspars dissolving at 920 °C provided crucial guidelines. The selected range from 1000 °C to 1300 °C is consistent with literature, especially considering porcelain's typical transformation temperatures, which are often above 1300 °C.

Our batch compositions presented in Table 1, were influenced by the ternary phase diagram at 1300 °C [12–14].

In alignment with this guidance and to remain within the advised range, we opted for a blend comprising 45 % kaolinitic clay, 30 % feldspar, and 25 % quartz. The chosen percentages aim to achieve specific physical properties in the final porcelain product. They're especially relevant to the sintering temperature of 1300 °C, ensuring optimal phase development and crystalline properties as detailed in Ref. [15].

3. Results and discussion

The electron microscope microstructure of the raw material granules DD2 which are in the form of rods Fig. 1(a), as for the quartz, the distribution of granules is almost regular Fig. 1(b). There are also several types, which differ by the nature and concentration of the impurities entering into their composition [16,17]. The quartz, the white stone originates from Algeria.

By XRD, every chemical and oxide found in DD2 was examined (Fig. 2) and in addition quartz, feldspars and automotive glass recovered by XRF analysis (Table 2):

The percentage of glassy phase in the ceramic (porcelain) can be determined by dissolving it in HF acid. This method, although destructive to the samples and regardless of the dangers associated with the use of this acid, is considered an easy method to use. The aim is to achieve a precise functionality, which follows the kinetics of dissolution of the material in solution. We ground the ceramic samples and passed them over a 125 μm diameter sieve. The samples were placed in a dilute solution of hydrofluoric acid at a concentration of (40–45) %, We attached the samples (with a similar weight of about 1 g) to a 125 ml beaker with HF solution, and measured the masses of the samples at different times (60, 45, 30, 15 and 120 min). The difference between the initial and final weight of the powder gives the weight loss that occurs during the attack time, the test is repeated in the same way and at different times, knowing that the hydrofluoric acid solution strongly attacks the glass phase, unlike the other phases. The results obtained were compared with a sample of control glass to verify the mechanism of the experiment [18].

Hydrofluoric acid attacks the glassy phase (amorphous) regularly and at a constant reaction rate. After the glassy phase is exhausted, it changes speed, which indicates that we have entered the crystalline phase. The shape of the glass changes its trend between the corresponding temperatures at time 60 and 120 min (Fig. 3), this is due to the decrease of the acid concentration and not to the lack of liquid phase due to the appearance of water in the dissociation equation products:

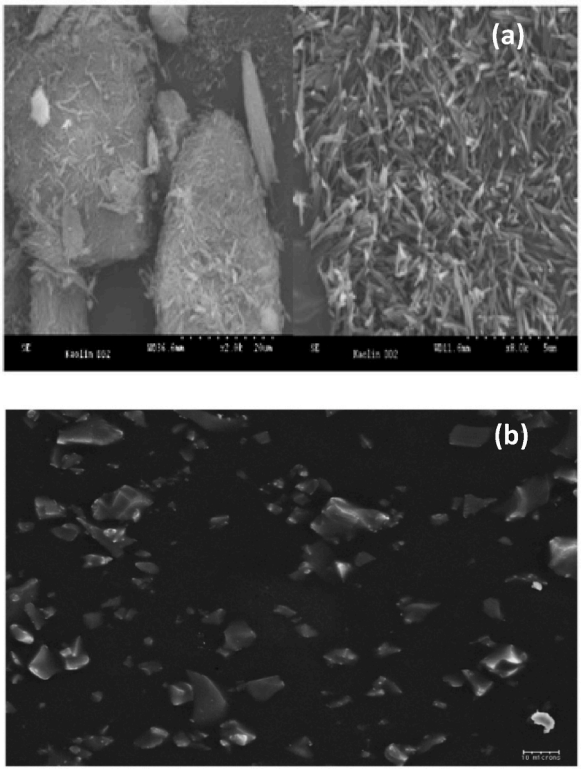

Fig. 1. SEM microstructures of raw Kaolin DD2 (a) and quartz grains (b).

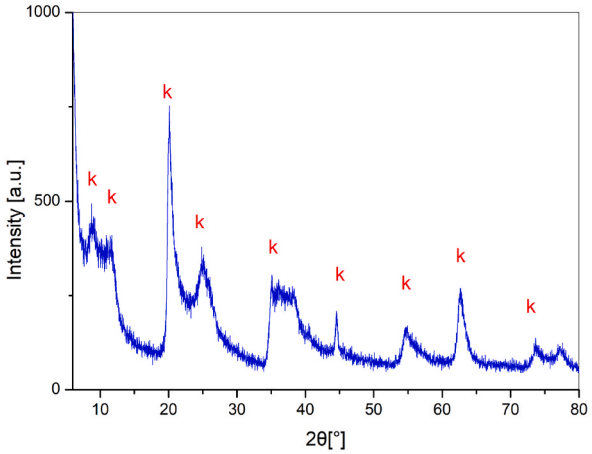

Fig. 2. X-ray diffraction spectra of raw Kaolin DD2.

Table 2
The composition of the weight ratios.

Oxides	Kaolin DD2 (%)	Quartz (%)	Feldspars (%)	Glass (%)
SiO_2	45.52	99.9	69	69.86
Al_2O_3	38.75	0.027	17.5	1.08
FeO_3	0.04	0.005	0.17	0.08
CaO	0.18	0.001	2.32	10
Na_2O	0.05	–	0.37	13.11
K_2O	0.03	0.002	10.22	0.03
MgO	–	0.001	–	1.55
P_2O_5	–	0.001	–	–
SO_3	–	–	0.16	0.38
TiO_2	–	0.0002	–	–
L.O.I	15.44	0.01	0.42	–

$$SiO_2 + 6HF \rightarrow SiF_6H_2 + 2H_2O$$

The mass loss percentage as a function of the ratio of glass to porcelain is presented in Fig. 4.
From this curve, the equation for the mass ratio of the glass phase as a function of the glass/porcelain ratio is derived (Eq. (1)):

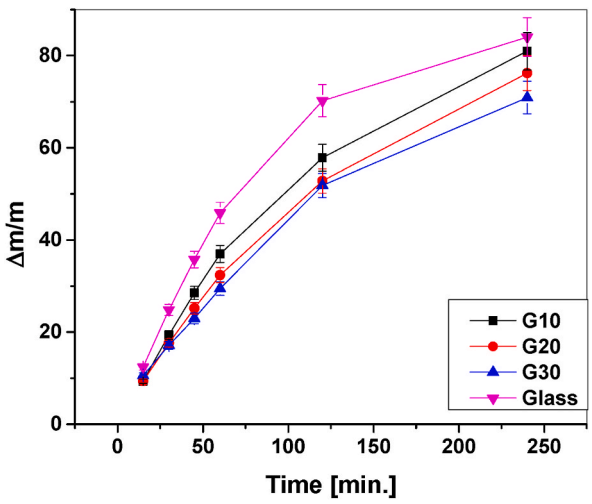

Fig. 3. Mass ratio as a function of time.

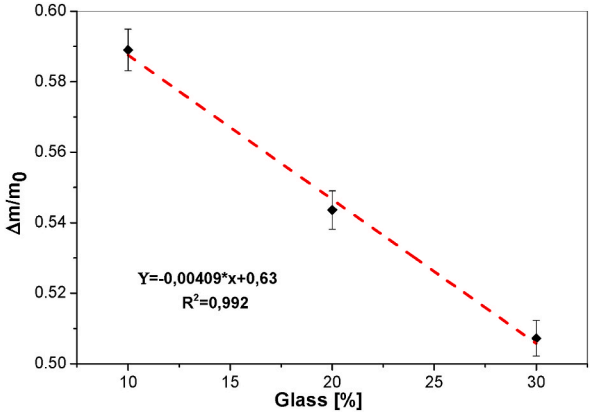

Fig. 4. The mass loss percentage as a function of the ratio of glass to porcelain.

$$F(k) = -0.00409k + 0.630 \quad \text{Eq. 1}$$

Equation F(k) is satisfied under the following conditions: (Sintering 2 h at 1000 °C).

Fig. 5 indicates a significant decrease in the diffraction lines of the anorthite phase was noticed at 1150 °C, which means its transformation into an amorphous phase. At 1100 °C, mullite diffraction lines begin to appear. As a result; we are witnessing transformations within the grains belonging to kaolin alone. As for the alumina grains, at this level, they have not begun to interact with the silicon oxide to form the secondary mullite, which begins to form at 1200 °C [19].

$$3(Al_2O_3.2SiO_2) \xrightarrow{1100^\circ C} 3Al_2O_3.2SiO_2 + 4SiO_2$$

Such as, $3Al_2O_3(2SiO_2)$; the primary mullite, as for the secondary mullite, it is formed from the association of 4SiO2 amorphous from the previous equation with Al2O3 for the formation of the secondary mullite. We also note the emergence of the protrusion of the vitreous phase gradually until reaching a maximum at 1300 °C, due to the fusion of quartz and anorthite [19].

Fig. 6; shows a noticeable increase in the intensity of the anorthite phase compared to that of the G00; due to the percentage of CaO present in the added recovered glass, but it decreases significantly at 1200 °C, which means its transformation has an amorphous phase. At 1100 °C, the diffraction lines of the primary mullite begin to appear, knowing that the primary mullite is a product of the

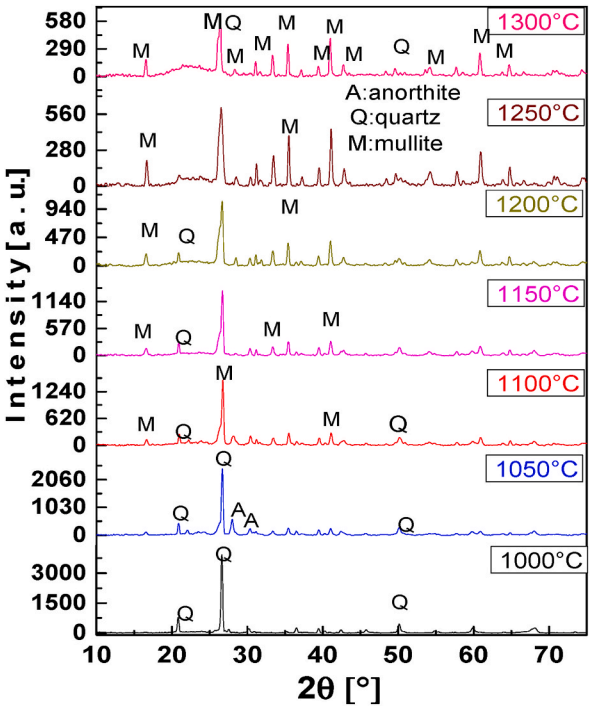

Fig. 5. X-ray diffraction spectra of G00 samples sintered at (1000, 1050, 1100, 1150, 1200, 1250 °C) and a constant sintering time of 120 min.

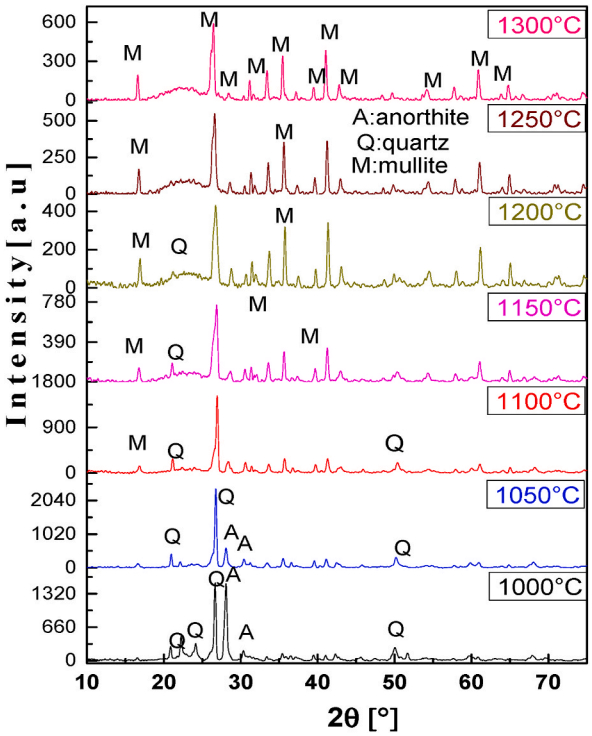

Fig. 6. X-ray diffraction spectra of G10 samples sintered at (1000, 1050, 1100, 1150, 1200, 1250 °C) and a constant sintering time of 120 min.

reactions of kaolinite. As for the alumina granules, they have not, at this point, begun to interact with the silicon oxide to form the secondary mulite, which begins to form at 1200 °C. Note the protrusion of the vitreous phase gradually until it reaches its maximum at 1300 °C, knowing that porcelain transforms at a temperature above 1300 °C into an amorphous phase (liquid phase).

At temperatures above 1150 °C the samples become spongy due to the availability of dissolved oxides in the medium, with an increase in the intensity of the anorthite peaks, due to the proportion of CaO considered in the added glass. In addition, the swelling of the vitreous phase at a temperature of 1150 °C increases sharply due to the fusion of quartz and anorthite Fig. 7.

Samples become spongy at temperatures above 1100 °C due to solvents. We also note that the intensity of the anorthite peaks have increased, although it begins to decrease due to its transformation into the liquid phase, besides quartz, which in turn has a high crystallization intensity and decreases with increasing processing temperature, as for the glassy phase, its protrusion increases until the samples melt (Fig. 8). For the calculation of the theoretical weight ratios for these phases; taking into account the water that enters into the chemical composition of the raw materials. The anorthite consists of 2 mol of SiO2 and 1 mol of Al_2O_3 in addition to 1 mol of CaO and since the lower weight percent in the G00 samples is due to CaO approximately (0.802633 g), the ratio of anorthite is 6.91 %. On the other hand, the mullite consists of 2 mol of silica and 3 mol of alumina (the small percentage is due to aluminum, approximately (28.17 g), the ratio of mullite is (39.21445 %). The highest percentage of quartz does not exceed 20 % (Table 3).

The findings demonstrated that the glass's dissolved oxides caused the substance to melt more quickly when it was added. Additionally, there is a variance in the samples' anorthite proportion, which is correlated with the presence of CaO, a high percentage has observed, particularly in the two samples G20 and G30, which contain a large percentage of glass due to the ease of its formation. As for the samples G00 and G10, we note that its percentage is low, and that the anorthite begins to melt at 1100 °C and to unite the aluminium atoms which were linked to it to form the secondary mullite at 1200 °C. The percentage of the vitreous phase increases; due to the dissolved silica and anorthite, where it reaches its highest percentage in pure porcelain theoretically around 70 % [20]. Similarly, an increase in the proportion of the mullite phase in various samples with the increase in temperature was observed, it stabilized at a temperature of 1100 °C in the two samples G00 and G10 then it rose to 1200 °C, this is mainly due to the formation of secondary mullite, which is formed from the silica remaining from the formation of the primary mullite and the aluminium contained in the feldspars (about 17 %). As for the G20 and G30 samples, only the primary mullite forms due to the lack of aluminium due to the replacement of feldspars by glass Fig. 9(a–d). We used Rietveld refinement method to obtain the chemical formula crystal system space group unit cell dimensions a, b, c and cell volume V for different phases of glass at 1150 °C, presented in Table 4.

4. Conclusion

The research aimed to assess the implications of substituting feldspar with recovered automotive glass during the sintering process of porcelain. Key findings include:

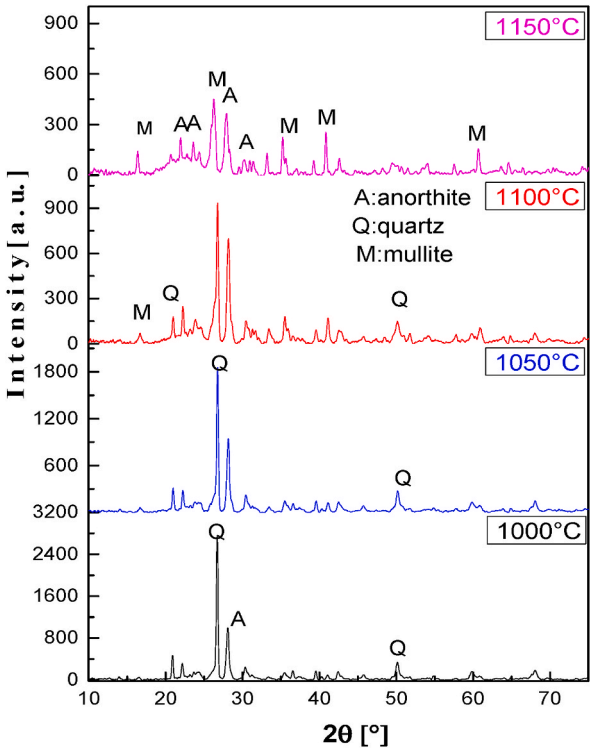

Fig. 7. X-ray diffraction spectra of G20 samples sintered at (1000, 1050, 1100, 1150, 1200, 1250 °C) and a constant sintering time of 120 min.

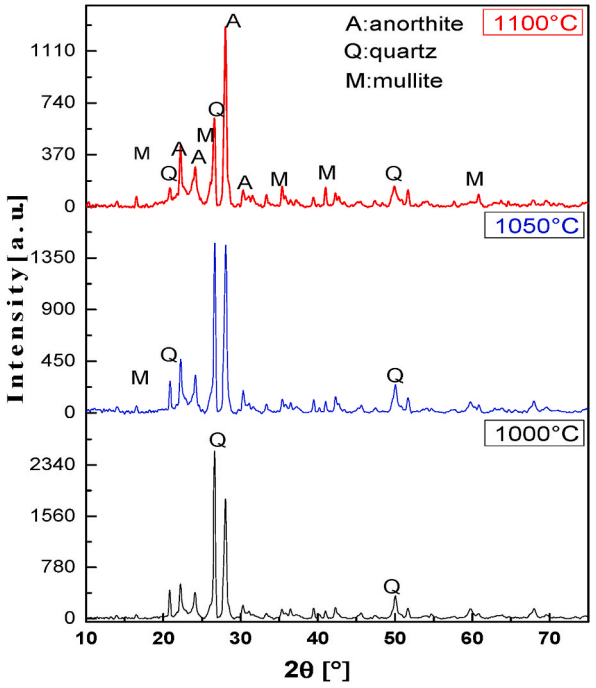

Fig. 8. X-ray diffraction spectra of G30 samples sintered at (1000, 1050, 1100, 1150, 1200, 1250 °C) and a constant sintering time of 120 min.

Table 3
Weight ratios and phase percentages for the different samples.

	Quartz (wt.%)	Mullite (wt.%)	Anorthite (wt.%)
G00	20	28.17	0.803
	20	39.21	6.91
G10	20	26.53	1.571
	20	36.93	13.52
G20	20	24.88	2.34
	20	34.64	20.13
G30	20	23.24	3.11
	20	32.36	26.74

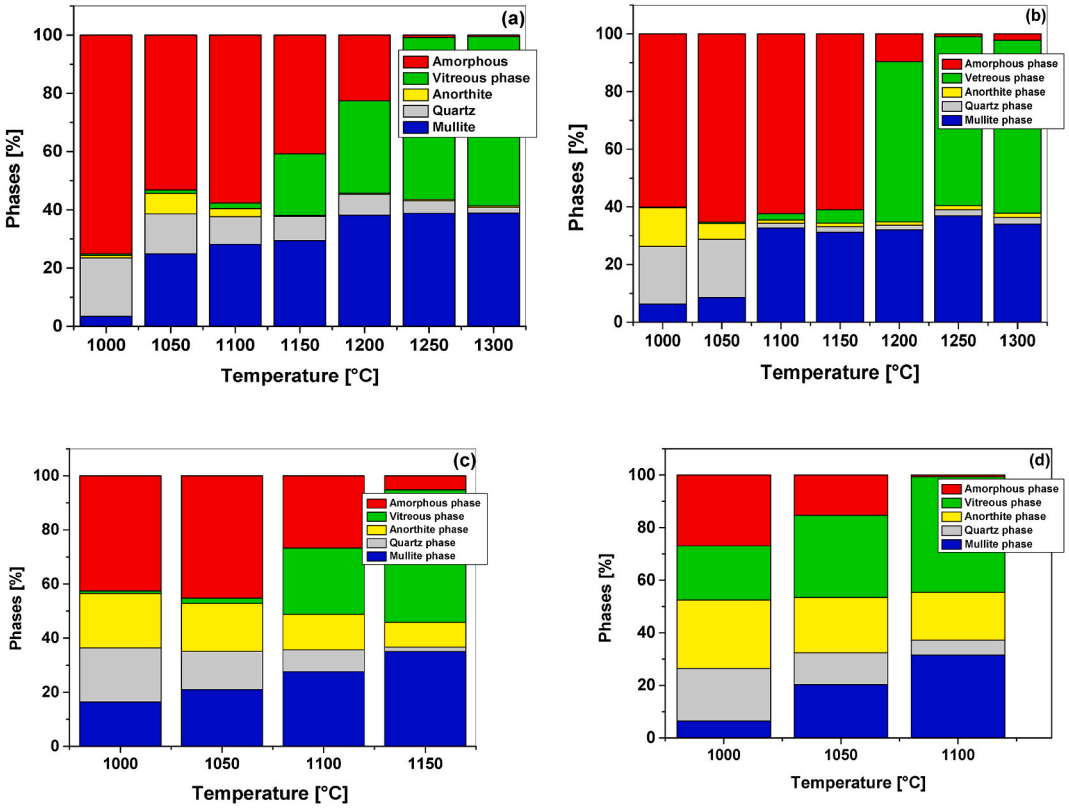

Fig. 9. The phase's appearance ratio versus of heat treatment for G00 (a), G10 (b), G20 (c) and G30 (d) samples.

- ✓ The inclusion of automotive glass notably hastened the melting of porcelain material because of the dissolved oxides it introduced. This is in line with observations that materials containing dissolved oxides, such as added glass, accelerate melting.
- ✓ A significant transformation was noted in the anorthite phase. Specifically, it transitioned into an amorphous phase at 1150 °C, suggesting potential changes in the porcelain's structural and visual characteristics.
- ✓ The emergence of mullite at 1100 °C due to kaolinite transformations underscores its possible contribution to boosting the thermal stability of porcelain.
- ✓ Temperatures exceeding 1150 °C made the samples porous.
- ✓ Through calculations, it was discerned that the anorthite ratio stood at 6.91 %, while mullite and quartz were at 39.21 % and less than 20 % respectively.
- ✓ These results have profound ramifications for the ceramics sector, especially in areas where feldspar importation is either costly or logistically cumbersome.
- ✓ The use of reclaimed automotive glass as a replacement presents both economic and ecological advantages. Nevertheless, more studies are needed to address the sponginess observed at elevated temperatures and to capitalize on the full advantages of this substitution in practical scenarios.

Table 4
The chemical formula crystal system space group unit cell dimensions a, b, c and cell volume V for different phases of glass.

	Reference			G00			G10			G20			G30 (at 1100 °C)		
phase	Anorthite	Quartz Low	Mullite	Anorthite	Quartz Low	Mullite	Anorthite	Quartz Low	Mullite	Anorthite	Quartz Low	Mullite	Anorthite	Quartz Low	Mullite
Reference code	98-008-6317 [21]	98-009-0145 [22,23]	98-006-6264 [24]	refinement results											
Chemical formula	$CaAl_2Si_2O_8$	SiO_2	$Al_6Si_2O_{13}$	$CaAl_2Si_2O_8$	SiO_2	$Al_6Si_2O_{13}$	$CaAl_2Si_2O_8$	SiO2	$Al_6Si_2O_{13}$	$CaAl_2Si_2O_8$	SiO_2	$Al_6Si_2O_{13}$	$CaAl_2Si_2O_8$	SiO_2	$Al_6Si_2O_{13}$
Crystal system	Triclinic	Hexagonal	Orthorhombic	Triclinic	Hexagonal	Orthorhombic	Triclinic	Hexagonal	Orthorhombic	Triclinic	Hexagonal	Orthorhombic	Triclinic	Hexagonal	Orthorhombic
Space group	P −1	P 31 2 1	P b a m	P −1	P 31 2 1	P b a m	P −1	P 31 2 1	P b a m	P −1	P 31 2 1	P b a m	P −1	P 31 2 1	P b a m
a(Å)±0.001	8.1750	4.916	7.5880	8.2	4.93	7.52	8.10	4.93	7.52	8.2	4.90	7.54	8.1	4.86	7.56
b(Å)±0.001	12.8730	4.916	7.6880	12.90	4.93	7.69	12.80	4.93	7.70	12.9	4.90	7.68	12.9	4.86	7.72
c(Å)±0.001	12.9019	5.409	2.8900	12.90	5.41	2.864	12.80	5.42	2.879	12.9	5.36	2.887	12.8	5.54	2.86
Alpha (°)	85.771	90	90	85.51	90	90	86.25	90	90	86.05	90	90	86.76	90	90
Beta (°)	81.137	90	90	81.90	90	90	73.06	90	90	81.25	90	90	81.69	90	90
Gamma (°)	88.72	120	90	88.85	120	90	89.65	120	90	88.61	120	90	89.38	120	90
Volume of cell ($Å^3$)	1337.81	113.21	168.59	1345.36	113.90	165.6	1315.30	114.15	166.73	1338.47	111.23	167.12	1334.97	113.41	167.08

Data availability

Data will be made available on request.

CRediT authorship contribution statement

A. Djemli: Project administration, Methodology, Investigation. **M.A. Ghebouli:** Funding acquisition, Formal analysis, Data curation, Conceptualization. **K. Bouferrache:** Supervision, Software, Resources, Project administration, Methodology, Investigation. **Y. Slimani:** Writing – review & editing, Writing – original draft, Visualization, Validation. **Mohamed A. Habila:** Resources, Project administration, Methodology. **Fatmi M:** Writing – original draft, Visualization, Validation, Supervision, Software. **T. Chihi:** Writing – review & editing, Writing – original draft, Visualization, Validation, Supervision, Software. **B. Ghebouli:** Writing – review & editing, Supervision, Project administration, Investigation. **Mika Sillanpää:** Writing – review & editing, Writing – original draft.

Declaration of competing interest

The authors declare that they have no known competing financial interests or personal relationships that could have appeared to influence the work reported in this paper.

Acknowledgements

This Work Was Funded by The Researchers Supporting Project Number (RSP2023R441), King Saud University, Riyadh, Saudi Arabia.

References

[1] D.W. Richerson, Modern Ceramic Engineering, Marcel Dekker, Inc, New York, 1992.
[2] R.B. Heimann, Classic and Advanced Ceramics: from Fundamentals to Applications, Wiley-VCH, 2010.
[3] D. Dumora, Techniques de l'ingénieur D274 (1982) 1–12.
[4] G. Yanyi, Raw materials for Making porcelain and the characteristics of porcelain Wares in north and south China in ancient times, Archaeometry 29 (1) (1987) 3–19.
[5] J.C. Echallier, S. Mery, L'évolution minéralogique et physico-chimique des céramiques au cours de la cuisson, applications archéologiques, approche expérimentale en laboratoire, Geologues 87 (1992) 64–70.
[6] P. Sciau, M. Werwerft, A. Vernhet, C. Bémont, Recherche sur les températures de cuisson et la nature des engobes des céramiques sigillées de la Graufesenque, Revue d'Archéométrie 16 (1992) 89–95.
[7] P. Rice, Pottery Analysis, a Sourcebook, second ed., University of Chicago Press, Chicago – London, 2015.
[8] R. Kreimeyer, Some notes on the firing colour of clay bricks, Appl. Clay Sci. 2 (2) (1987) 175–183.
[9] A. Aras, The change of phase composition in kaolinite- and illite-rich clay-based ceramic bodies, Appl. Clay Sci. 24 (2004) 257–269.
[10] E.A. Carter, M.L. Wood, D. De Waal, G.M. Edwards, Porcelain shards from Portugueuse wrecks: Raman spectroscopic analysis of archaeological ceramics, Heritage Science 5 (2017) 130–139.
[11] Y. Leon, C. Lofrumento, A. Zoppi, R. Carles, E.M. Castellucci, Ph Sciau, Micro-Raman investigation of terra sigillata slips: a comparative study of central Italuan and southern Gaul production, J. Raman Spectrosc. 41 (11) (2010) 1550–1555.
[12] S. Yilmaz, Z.E. Erkmen, Creep of hard porcelain during firing, Am. Ceram. Soc. Bull. 86 (8) (2007) 9301–9305.
[13] Y. Sawadogo, L. Zerbo, M. Sawadogo, M. Seynou, M. Gomina, P. Blanchart, Characterization and use of raw materials from Burkina Faso in porcelain formulations, Results in Materials 6 (2020), 100085.
[14] A.L. Stuijts, Microstructure of ceramic materials, Proceedings of a Symposium (1963) 125.
[15] K. Dana, S. Das, S.K. Das, Effect of substitution of fly ash for quartz in triaxial kaolin–quartz–feldspar system, J. Eur. Ceram. Soc. 24 (2004) 3169–3175.
[16] H.H. Murray, Occurrences, processing and applications of kaolins, bentonites, palygorskitesepiolite, and common clays, Applied clay mineralogy 2 (2006) 1–180.
[17] E. Karamanova, G. Avdeev, A. Karamanov, Ceramics from blast furnace slag, kaolin and quartz, J. Eur. Ceram. Soc. 31 (6) (2011) 989–998.
[18] K.R. Mikeska, S.J. Bennison, Corrosion of alumina in aqueous hydrofluoric acid, J. Am. Ceram. Soc. 82 (12) (1999) 3561–3566.
[19] C.Y. Chen, G.S. Lan, W.H. Tuan, Preparation of mullite by the reaction sintering of kaolinite and alumina, J. Eur. Ceram. Soc. 20 (2000) 2519–2525.
[20] K. Tabit, H. Hajjou, M. Waqif, L. Saàdi, Effect of CaO/SiO2 ratio on phase transformation and properties of anorthite-based ceramics from coal fly ash and steel slag, Ceram. Int. 46 (2020) 7550–7558.
[21] P.E. Tomaszewski, Golden book of phase transitions, Wroclaw (2002) 11–123.
[22] F. Alessandro, Accuracy of XRPD QPA using the combined Rietveld–RIR method, J. Appl. Crystallogr. 33 (2000) 267–278.
[23] A. Djemli, H. Belhouchet, A. Faci, M.A. Ghebouli, K. Bouferrache, Y. Slimani, T. Chihi, B. Ghebouli, M. Fatmi, Norah Algethami, S. Alomairy, Sustainable porcelain ceramics production using local raw materials and recycled automotive glass, Mod. Phys. Lett. B 37 (2023), 2450064.
[24] C.T. Prewitt, R.K. McMullan, R. J Angel, Substructure and superstructure of mullite by neutron diffraction, Am. Mineral. 71 (1986), 1476-148.